A Model-Based Impedance Control of a 6-dof Electrohydraulic Stewart Platform

Ioannis Davliakos and Evangelos Papadopoulos

Abstract—**In this paper, a model-based impedance controller for a six-degree-of-freedom (dof) electrohydraulic Stewart platform mechanism is developed. Rigid body and electro-hydraulic models, including servovalve models are employed and described by a set of integrated system equations. Friction and leakage of hydraulic elements are also included. The developed controller uses the system dynamic and hydraulic model to yield servovalve currents. The control law consists of two signals, a feedback and a feedforward signal. An impedance filter modifies the desired trajectory according to a specified behaviour. The modified trajectory is fed to the system model to reduce the effects of the nonlinear hydraulic dynamics. Simulations with typical desired trajectories are presented and a good performance of the controller is obtained.**

I. Introduction

THE original six-Degree-of-Freedom (dof) Stewart-Gough platform was developed in 1954 [1], [2]. In 1965, the prototype parallel mechanism was used as a 6-dof motion platform for a flight simulator [3]. Since then, a number of studies on this mechanism and its variations have been published, i.e. [4]. The mechanism can be driven electrically or electrohydraulically. The kinematics and dynamics of the Stewart platform have been studied by many researchers [5]–[8]. However, actuation dynamics have not been considered. Although electrohydraulic Stewart platforms have been used extensively, little published work on their full dynamics including actuation and control, exists.

Impedance control is considered to be an active compliant motion control, mainly required for industry applications and in cases force interactions with the environment, i.e. CNC, milling machines, etc. [18], [20]. Such a controller offers safety and flexibility and is preferred over other control techniques.

Hydraulics science combined with controls, has given new thrust to hydraulics applications. The main reasons why hydraulics are preferred to electromechanical drives in some industrial and mobile applications, include their ability to produce large forces at high speeds, their high durability and stiffness, and their rapid response [9], [10]. Hydraulic regimes differ from electromechanical ones, in that the force or torque output is not proportional to actuator current and therefore, hydraulic actuators cannot be modeled as force/ torque sources, but as controlled impedances. As a result, controllers that have been designed for robot control, assuming the capability of setting actuator force/ torque, cannot be used here.

Control techniques are used to compensate for the nonlinearities of electrohydraulic servosystems. Nonlinear adaptive control techniques for hydraulic servosystems have been proposed by researchers assuming linearization [11] and backstepping [12], approaches. A robust force controller design based on the nonlinear Quantitative Feedback Theory, has been implemented on an industrial hydraulic actuator, taking into account system and environmental uncertainties [13].

A unified approach to the control of an electric manipulator applicable to free motions, kinematically constrained motions, and dynamic interaction between the manipulator and its environment has been examined in [14]. Techniques for implementing a desired manipulator impedance and for choosing the impedance appropriate to a given application using optimization theory were presented [14]. Two spatio-geometric methods for controlling the mechanical impedance for an electromechanically driven Gough-Stewart class of parallel platforms were presented [15]. The first was based on global potential energy functions while the second used the exponential map to associate finite displacements of the platform from equilibrium with twist displacements.

A model-based, feedforward-feedback impedance controller of hydraulic servosystems for high-performance hydraulic joints has been proposed, in which an impedance filter adjusts the desired trajectory according to a prescribed behaviour in free space and in contact [16], [17]. Similar work has been presented in [18], where a position-based impedance controller for an industrial hydraulic manipulator is developed. Further, impedance controllers have been studied and implemented on teleoperated hydraulic servosystems for heavy duty works, [19], [20].

In this paper, a model-based impedance controller for a six-dof electrohydraulic Stewart platform with symmetric

Manuscript received October 16, 2006.

Support by the EPAN Cooperation Program 4.3.6.1 (Greece-Poland) of the Hellenic General Secretariat for Research and Technology and the NTUA Senator Committee of Basic Research Programme "Protagoras", R.C. No. 10, is acknowledged.

I. Davliakos is with the National Technical University of Athens, Greece (e-mail: gdavliak@central.ntua.gr).

E. Papadopoulos is with the National Technical University of Athens (NTUA), Greece (corresponding author, phone: +(30) 210-772-1440; fax: +(30) 210-772-1455; e-mail: egpapado@central.ntua.gr).

joint locations is developed. Dynamic models are used that describe the rigid body equations of the Stewart platform and the hydraulics dynamics of its actuation system. In contrast to other approaches, here, servovalve models and friction are included in the model. The developed control scheme employs rigid body and actuation dynamics and yields the servovalve input current vector, in analytical form. The control law consists of two signals, a feedback and a feedforward signal. An impedance filter modifies the desired trajectory according to a specified behaviour. The modified trajectory is fed to the system model to reduce the effects of the nonlinear hydraulic dynamics. The performance of the developed controller is illustrated using typical trajectories. The proposed methodology can be extended to electrohydraulic serial or closed-chain manipulators and simulators.

II. System Modeling

In this section, the dynamic model of a 6-dof electro-hydraulic Stewart platform servomechanism [3] is examined. This is a six dof closed kinematic chain mechanism consisting of a fixed base and a moving platform with six linear actuators supporting it. The mechanism is illustrated schematically in Fig. 1.

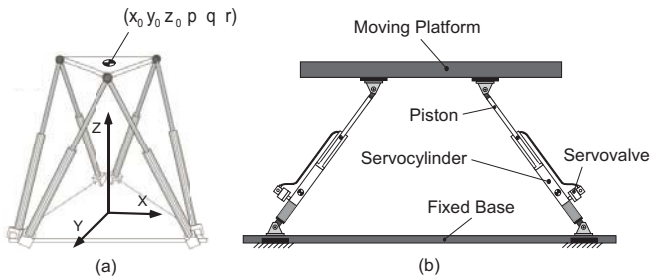

Fig. 1. (a) Schematic view of a six-dof Stewart Platform, (b) Drawing showing two of the six servoactuators.

A. Mechanical Dynamics

A full servosystem model includes the moving mass equation of motion. This system provides a relation between the actuator torques/forces and the resulting motion. The equation of motion for the Stewart platform system is derived applying a Lagrangian formulation and is written as

$$\mathbf{M}(\mathbf{x})\,\ddot{\mathbf{x}} + \mathbf{V}(\mathbf{x},\dot{\mathbf{x}}) + \mathbf{G}(\mathbf{x}) + \mathbf{F}_{fr}(\dot{\mathbf{x}}) = \boldsymbol{\tau} \tag{1}$$

where $\mathbf{x} = \left(x_0,\, y_0,\, z_0,\, p,\, q,\, r\right)^{\mathrm{T}}$ is the 6×1 vector of the platform generalized coordinates, see Fig. 1(a), x_0, y_0, z_0, are the platform center of mass Cartesian coordinates, p, q, r are the platform Euler angles, $\mathbf{M}(\mathbf{x})$ is the 6×6 positive definite mass matrix of the system, the 6×1 vector $\mathbf{V}(\mathbf{x},\dot{\mathbf{x}})$ represents forces/ torques arising from centrifugal and Coriolis forces, the 6×1 vector $\mathbf{G}(\mathbf{x})$ represents torques due to gravity, $\mathbf{F}_{fr}(\dot{\mathbf{x}})$ is the 6×1 vector of the forces/ torques due to friction, and $\boldsymbol{\tau}$ is the 6×1 vector of the generalized applied forces.

Equation (1) can be further extended using the transformation between mechanism actuator forces and the generalized applied forces, [4], which is given by,

$$\boldsymbol{\tau} = \mathbf{J}^{\mathrm{T}}\mathbf{F}_p \tag{2}$$

where $\mathbf{J}$ is the Jacobian 6×6 matrix of the system, and $\mathbf{F}_p$ is a 6×1 vector representing actuator forces given by,

$$\mathbf{F}_p = \left(F_{p,1},\, F_{p,2},\, ...,\, F_{p,6}\right)^{\mathrm{T}} \tag{3}$$

where $F_{p,j}$, $j = 1,2,...,6$ are individual hydraulic forces acting on the platform.

Using mechanism inverse kinematics, the platform Cartesian motion described by (1) can be transformed to its joint space and written as,

$$\mathbf{M}^*(\mathbf{x})\,\ddot{\boldsymbol{\ell}} + \mathbf{V}^*(\mathbf{x},\dot{\mathbf{x}}) + \mathbf{G}^*(\mathbf{x}) + \mathbf{F}^*_{fr}(\dot{\boldsymbol{\ell}}) = \mathbf{F}_p \tag{4}$$

where $\boldsymbol{\ell} = \left(\ell_1,\, \ell_2,\, ...,\, \ell_6\right)^{\mathrm{T}}$ is the 6×1 vector of the mechanism actuator lengths, $\mathbf{M}^*(\mathbf{x})$ is a 6×6 positive definite mass matrix, $\mathbf{V}^*(\mathbf{x},\dot{\mathbf{x}})$ is a 6×1 vector that contains the centrifugal and Coriolis forces, $\mathbf{G}^*(\mathbf{x})$ is a 6×1 gravity forces vector, and $\mathbf{F}^*_{fr}(\dot{\boldsymbol{\ell}})$ is a 6×1 vector that contains joint space frictional forces. The terms $\mathbf{M}^*(\mathbf{x})$, $\mathbf{V}^*(\mathbf{x},\dot{\mathbf{x}})$ and $\mathbf{G}^*(\mathbf{x})$ are given, respectively by,

$$\mathbf{M}^*(\mathbf{x}) = [\mathbf{J}(\mathbf{x})^{\mathrm{T}}]^{-1}\,\mathbf{M}(\mathbf{x})\,\mathbf{J}(\mathbf{x})^{-1} \tag{5a}$$

$$\mathbf{V}^*(\mathbf{x},\dot{\mathbf{x}}) = [\mathbf{J}(\mathbf{x})^{\mathrm{T}}]^{-1}\left[\mathbf{V}(\mathbf{x},\dot{\mathbf{x}}) - \mathbf{M}(\mathbf{x})\,\dot{\mathbf{J}}(\mathbf{x},\dot{\mathbf{x}})\cdot\dot{\mathbf{x}}\right] \tag{5b}$$

$$\mathbf{G}^*(\mathbf{x}) = [\mathbf{J}(\mathbf{x})^{\mathrm{T}}]^{-1}\mathbf{G}(\mathbf{x}) \tag{5c}$$

A number of methods exists, that can be used to model the friction vector $\mathbf{F}^*_{fr}(\dot{\boldsymbol{\ell}})$, [21]. A widely used method models friction as,

$$\mathbf{F}^*_{fr}(\dot{\boldsymbol{\ell}}) = \mathbf{F}^*_v(\dot{\boldsymbol{\ell}}) + \mathbf{F}^*_c(\dot{\boldsymbol{\ell}}) + \mathbf{F}^*_s \tag{6}$$

where $\mathbf{F}^*_v(\dot{\boldsymbol{\ell}})$, $\mathbf{F}^*_c(\dot{\boldsymbol{\ell}})$ and $\mathbf{F}^*_s$ are the viscous, Coulomb and static friction vector respectively, with elements,

$$F^*_{v,j}(\dot{\ell}_j) = \begin{cases} 0, & \dot{\ell}_j = 0, \quad j = 1,2,...,6 \\ b_j\dot{\ell}_j, & \dot{\ell}_j \neq 0, \quad j = 1,2,...,6 \end{cases} \tag{7a}$$

$$F^*_{c,j}(\dot{\ell}_j) = \begin{cases} 0, & \dot{\ell}_j = 0, \quad j = 1,2,...,6 \\ F_{c0,j}\,sgn(\dot{\ell}_j), & \dot{\ell}_j \neq 0, \quad j = 1,2,...,6 \end{cases} \tag{7b}$$

$$F^*_{s,j} = \begin{cases} F_{ext,j}, & |F_{ext,j}| < F_{s0,j},\ \dot{\ell}_j = 0,\ \ddot{\ell}_j = 0,\ j = 1,2,...,6 \\ F_{s0,j}\,sgn(F_{ext,j}), & |F_{ext,j}| > F_{s0,j},\ \dot{\ell}_j = 0,\ \ddot{\ell}_j \neq 0,\ j = 1,2,...,6 \\ 0, & \dot{\ell}_j \neq 0,\ \ j = 1,2,...,6 \end{cases} \tag{7c}$$

where b_j is the j[th] parameter for viscous friction element, $F_{c0,j}$ is the j[th] parameter for Coulomb friction element, $F_{ext,j}$ is the j[th] external force element, $F_{s0,j}$ is the j[th] breakaway force element and

$$sgn(\dot{\ell}_j)=\begin{cases}+1, & \dot{\ell}_j>0, \quad j=1,2,...,6\\ 0, & \dot{\ell}_j=0, \quad j=1,2,...,6\\ -1, & \dot{\ell}_j<0, \quad j=1,2,...,6\end{cases} \tag{8}$$

For control purposes, determination of the six forces acting on the platform is considered next. These are the net platform actuation forces that can be measured via force sensors, e.g. [25], or computed by,

$$\mathbf{F}_{act}=\mathbf{M}_{pl}(\mathbf{x})\ddot{\boldsymbol{\ell}}+\mathbf{V}_{pl}(\mathbf{x},\dot{\mathbf{x}})+\mathbf{G}_{pl}(\mathbf{x}) \tag{9}$$

where $\mathbf{M}_{pl}$ is the 6×6 positive definite mass matrix of the platform, $\mathbf{V}_{pl}$ represents forces/ torques arising from centrifugal and Coriolis forces on the platform, and $\mathbf{G}_{pl}$ represents platform forces/ torques due to gravity.

B. Hydraulic Dynamics

The electrohydraulic actuation servosystem of the platform consists of pistons, servovalves, controllers, sensors and a hydraulic power supply. Next, hydraulic models of electro-hydraulic servosystem major components are introduced.

Hydraulic supplies include pumps that are usually constant pressure piston pumps, driven by induction electric motors. Therefore, a pump is modelled as a constant pressure source. Further, they may include accumulators for filtering pressure pulsations from the pump, but also for allowing the use of smaller rating pumps by providing additional flow when needed. Such an accumulator, is modelled as a hydraulic capacitor [22].

A single rod hydraulic servocylinder is illustrated schematically in Fig. 2. The equations relating mechanical to hydraulic variables are described by,

$$Q_1=A_1\dot{\ell}+C_1\dot{p}_1+G_{p,in}(p_1-p_2) \tag{10a}$$

$$Q_2=A_2\dot{\ell}-C_2\dot{p}_2+G_{p,in}(p_1-p_2) \tag{10b}$$

$$A_1p_1-A_2p_2=F_p \tag{10c}$$

$$F_{act}=F_p-F_{fr,p} \tag{10d}$$

where Q_1, Q_2 are the flows through the two cylinder chamber ports, p_1, p_2 are the chamber pressures, A_1 is the piston side area, A_2 is the rod side area, C_1, C_2 are the fluid capacitances in the cylinder chambers, $G_{p,in}$ represents the cylinder internal leakage conductance, ℓ is the total length of actuator, F_p is the hydraulic force, $F_{fr,p}$ is the actuator friction force, and F_{act} is the net actuator output force. In the case of a hydraulic cylinder with a double rod, the two areas A_1 and A_2 are equal and therefore, (9) are simplified.

Control of a hydraulic system is achieved through the use of servovalves, see Fig. 3(a). Only the resistive effect of a valve is considered here, since their natural frequency is much higher than that of the mechanical load. It is also assumed that the geometry of the valve is ideal, e.g. the valve has sharp edges and zero cross leakage, [23], [24].

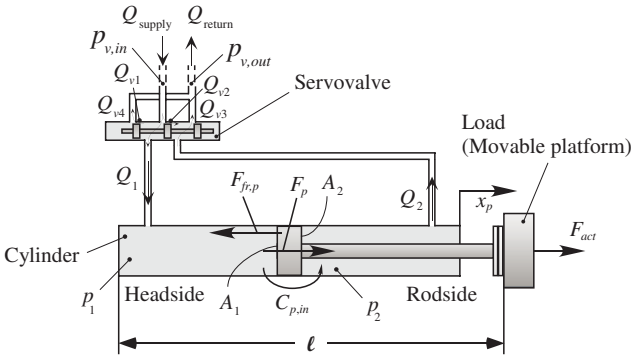

Fig. 2. Schematic model of a hydraulic servoactuator.

A typical hydraulic servovalve consists of four symmetric and matched servovalve orifices making up flow paths through four nonlinear resistors, modulated by the input voltage, see Fig. 3(a). Thereby, the servovalve is modeled as the hydraulic equivalent of a Wheatstone bridge, see Fig. 3(b). When the servovalve input current is positive, $i>0$, flow passes through the orifices 1 and 3 (path $P-A-B-T$), and flow leakages exist in the valve orifices 2 and 4. Similarly, when the servovalve input current is negative, $i<0$, flow passes through the path $P-A-B-T$, and flow leakages exist in the valve orifices 1 and 3.

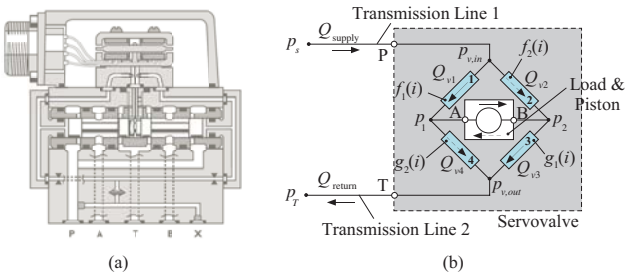

Fig. 3. Schematic model of hydraulic servovalve.

This model is described by,

$$Q_{v1}=f_1(i,C_d,\rho)\sqrt{p_{v,in}-p_1} \tag{11a}$$

$$Q_{v2}=f_2(i,C_d,\rho)\sqrt{p_{v,in}-p_2} \tag{11b}$$

$$Q_{v3}=g_1(i,C_d,\rho)\sqrt{p_2-p_{v,out}} \tag{11c}$$

$$Q_{v4}=g_2(i,C_d,\rho)\sqrt{p_1-p_{v,out}} \tag{11d}$$

where Q_{v1}, Q_{v2}, Q_{v3} and Q_{v4} are the servovalve flows through the orifices 1, 2, 3 and 4, respectively, $p_{v,in}$ and

$p_{v,out}$ are the input and output servovalve pressure of the servosystem, correspondingly, i is the servovalve motor current (control command), and $f_1(i,C_d,\rho)$, $f_2(i,C_d,\rho)$, $g_1(i,C_d,\rho)$ and $g_2(i,C_d,\rho)$ are nonlinear functions in the servovalve motor current, the discharge coefficient C_d and the mass density of the fluid, ρ. In general, the discharge coefficient is a function of the *Reynolds* number and valve geometry. However, fluid density and Reynolds dependencies are weak for turbulent flow and therefore only the current dependency is significant here, [9]; therefore, the functions $f_1(i,C_d,\rho)$, $f_2(i,C_d,\rho)$, $g_1(i,C_d,\rho)$, and $g_2(i,C_d,\rho)$ are reduced to $f_1(i)$, $f_2(i)$, $g_1(i)$ and $g_2(i)$, correspondingly. Because of servovalve symmetry, the current functions are given by,

$$f_1(i) = g_1(i) = f_2(-i) = g_2(-i) \tag{12a}$$

$$f_2(i) = g_2(i) = f_1(-i) = g_1(-i) \tag{12b}$$

Our experimental results showed that it is a good approximation to assume that these functions are linear functions of the input current, when flow passes through the main path, and have a constant value when flow passes through the leakage flow path [25]. For instance, when $i > 0$, the main flow path passes through the orifices 1 and 3 and therefore the functions of (11) are written as,

$$f_1(i) = g_1(i) = K_1 i + K_{0,1} \tag{13a}$$

$$f_2(i) = g_2(i) = K_{0,1} \tag{13b}$$

where K_1 and $K_{0,1}$ are positive constants, which correspond to the main and leakage valve flow paths.

The K_1 and $K_{0,1}$ constants for a two-land-four-way spool MOOG G761-3004 Series high-performance servovalve were experimentally computed and the results are depicted in Fig. 4 [25].

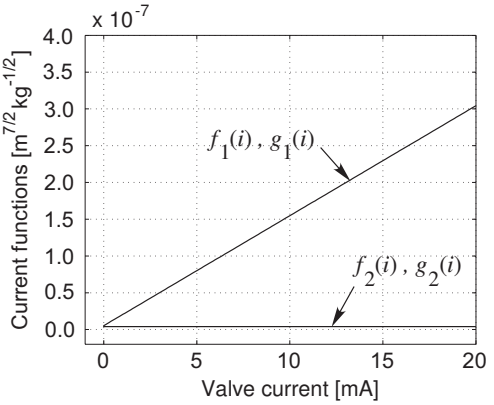

Fig. 4. Servovalve current functions in main and leakage path.

If leakage flows in servovalve and cylinder chamber are neglected, the flows through the orifices of the servovalve described by (11a,c) are equal to the flows through cylinder chamber ports, see (10a,b), and are written as,

$$Q_{v1} = Q_1 = A_1 \dot{\ell} + C_1 \dot{p}_1 \tag{14a}$$

$$Q_{v3} = Q_2 = A_2 \dot{\ell} - C_2 \dot{p}_2 \tag{14b}$$

Further, the combination of the continuity equation to each of the piston chambers yields, [9],

$$V_t (4\beta_e)^{-1} \Delta\dot{p}_L = Q_L - (A_1 - A_2)\dot{\ell} \tag{15}$$

where V_t is the total volume of fluid under compression in both chambers, β_e is the effective bulk modulus of the fluid, $\Delta p_L = p_1 - p_2$ is the piston pressure drop and Q_L is the load flow, which is given by, [9],

$$Q_L = F(i)\sqrt{(p_s - sgn(i)\Delta p_L)/2} \tag{16}$$

where $F(i)$ represents the servovalve current functions, i.e.,

$$F(i) = \begin{cases} f_1(i), & i > 0 \\ f_2(i), & i < 0 \end{cases} \tag{17}$$

Hydraulic hoses of the 6-dof electrohydraulic servosystem are modeled as compressible hydraulic lines, [22]. The equations that describe the hose dynamics are given by,

$$p_{l,in} - p_{l,m} = R\, Q_{l,in} \tag{18a}$$

$$\dot{Q}_{l,out} = (p_{l,m} - p_{l,out}) \cdot I^{-1} \tag{18a}$$

$$\dot{p}_{l,m} = (Q_{l,in} - Q_{l,out}) \cdot C^{-1} \tag{18b}$$

where $p_{l,in}$, $p_{l,out}$ and $p_{l,m}$ are the hose pressures at its input, output and a middle point respectively, $Q_{l,in}$, $Q_{l,out}$ are the flows through the hose at its input and output correspondingly, and the hose parameters R, I, C are the resistance, inertance and capacitance, respectively of the hydraulic line.

C. Integrated System Equations

The hydraulic and load dynamic response of the 6-dof Stewart platform can be described by integrated system equations derived using a systems approach, such as the Linear Graph, [22], or Bond Graph methods, [26]. To this end, one needs to provide expressions transforming pressure differences to forces, see (9c), and velocities to flows, see (10a,b). In general, the integrated hydraulic and mechanical load dynamics are described by nonlinear equations,

$$\begin{aligned} \dot{\boldsymbol{x}} &= \boldsymbol{f}(\boldsymbol{x}) + \boldsymbol{g}(\boldsymbol{x})\boldsymbol{u} \\ \boldsymbol{y} &= \boldsymbol{h}(\boldsymbol{x}), \qquad \boldsymbol{x}_0 = \boldsymbol{x}(t_0) = \boldsymbol{x}(\boldsymbol{0}) \end{aligned} \tag{19}$$

where $\boldsymbol{x}$ is a state column vector, $\boldsymbol{x}_0$ is the initial state

column vector for initial time $t_0 = 0$, $\boldsymbol{u}$ is the input column vector, $\boldsymbol{y}$ is the output column vector and, $\boldsymbol{f}(\boldsymbol{x})$, $\boldsymbol{g}(\boldsymbol{x})$, and $\boldsymbol{h}(\boldsymbol{x})$ are nonlinear functions.

Here, the Linear Graph method is applied. The linear graph of the full model of the 6-dof hydraulic servosystem is depicted in Fig. 5.

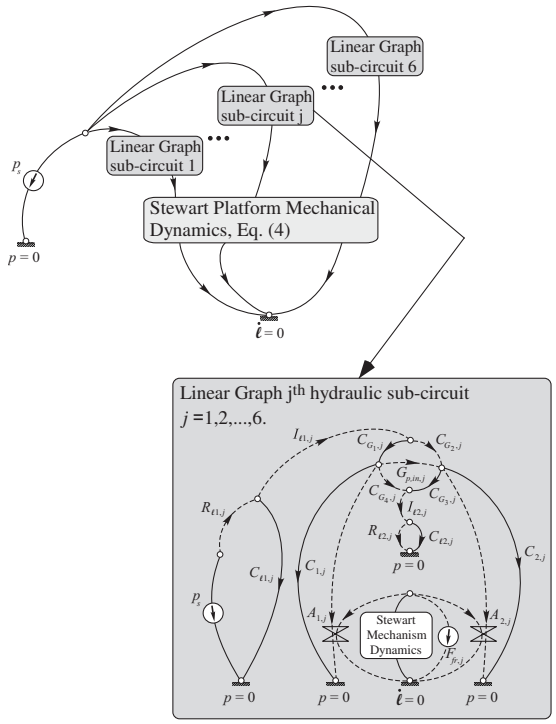

Fig. 5. Full linear graph of the 6-dof electrohydraulic Stewart platform model.

The application of continuity and compatibility laws, along with individual elements equations, leads to a set of 48 nonlinear first order differential equations, in the form of (19), as follows,

$$\dot{p}_{1,j} = [Q_{I,\ell 1} - Q_{v2}(i) - Q_{v4}(i) - G_{p,in}\cdot(p_1 - p_2) - A_1 v]\cdot C_1^{-1}\big|_j, \quad j=1,2,...,6 \tag{20a}$$

$$\dot{p}_{2,j} = [Q_{v2}(i) + Q_{v4}(i) - Q_{I,\ell 2} + G_{p,in}\cdot(p_1 - p_2) + A_2 v]\cdot C_2^{-1}\big|_j, \quad j=1,2,...,6 \tag{20b}$$

$$\dot{p}_{C,\ell 1,j} = [(p_s - p_{C,\ell 1})R_{\ell 1}^{-1} - Q_{I,\ell 1}]\cdot C_{\ell 1}^{-1}\big|_j, \quad j=1,2,...,6 \tag{20c}$$

$$\dot{p}_{C,\ell 2,j} = [Q_{I,\ell 2} - (p_{C,\ell 2} - p_T)R_{\ell 2}^{-1}]\cdot C_{\ell 2}^{-1}\big|_j, \quad j=1,2,...,6 \tag{20d}$$

$$\dot{Q}_{I,\ell 1,j} = [p_{C,\ell 1} - p_1 - \Delta p_{G_1}(i)]\cdot I_{\ell 1}^{-1}\big|_j, \quad j=1,2,...,6 \tag{20e}$$

$$\dot{Q}_{I,\ell 2,j} = [p_2 - p_{C,\ell 2} - \Delta p_{G_3}(i)]\cdot I_{\ell 2}^{-1}\big|_j, \quad j=1,2,...,6 \tag{20f}$$

$$\dot{v}_j = [\mathbf{m}^*_-]\big|_j \cdot (\mathbf{F}_p - \mathbf{V}^* - \mathbf{G}^* - \mathbf{F}^*_{fr}), \quad j=1,2,...,6 \tag{20g}$$

$$\dot{\ell}_j = v_j \tag{20h}$$

where $Q_{I,\ell 1,j}$, $Q_{I,\ell 2,j}$ are the j[th] flows in the j[th] hydraulic pressure and return line correspondingly, p_s, p_T are the power supply and return pressure of the servosystem, respectively, $p_{C,\ell 1,j}$, $p_{C,\ell 2,j}$ are correspondingly the j[th] pressures of j[th] hydraulic power and return line regarding with the lines' capacitances, $I_{\ell 1,j}$, $R_{\ell 1,j}$, $C_{\ell 1,j}$ are the j[th] inertance, resistance and capacitance of j[th] hydraulic power line respectively, $I_{\ell 2,j}$, $R_{\ell 2,j}$, $C_{\ell 2,j}$ are the j[th] inertance, resistance and capacitance of j[th] hydraulic return line respectively, v_j is the velocity of the j[th] piston, which is corresponded to the j[th] element of the vector, $[\mathbf{m}^*_-]\big|_j$ is a 1×6 row-matrix which corresponds to the j[th] line of the matrix $(\mathbf{M}^*)^{-1}$, and $\Delta p_{G_1}(i)\big|_j$, $\Delta p_{G_3}(i)\big|_j$ are the j[th] pressure drops of the j[th] servovalve orifices 1 and 3 respectively, which are determined using the flow continuity laws, along with actuator and servovalve elements equations, and given by,

$$\Delta p_{G_1}(i)\big|_j = \{[f_1^2(i) - f_2^2(i)]^{-1}\cdot[Q_{I,\ell 1} f_1(i) - f_2(i)\cdot \sqrt{Q_{I,\ell 1}^2 + [f_1^2(i) - f_2^2(i)]\cdot(p_1 - p_2)}]\}^2\Big|_j, \; j=1,...,6 \tag{21a}$$

$$\Delta p_{G_3}(i)\big|_j = \{[g_1^2(i) - g_2^2(i)]^{-1}\cdot[Q_{I,\ell 2}\, g_1(i) - g_2(i)\cdot \sqrt{Q_{I,\ell 2}^2 + [g_1^2(i) - g_2^2(i)]\cdot(p_1 - p_2)}]\}^2\Big|_j, \; j=1,...,6 \tag{21b}$$

Further, using the flow continuity laws, along with hydraulic lines and servovalve elements equations, the flows $Q_{v2,j}(i)$ and $Q_{v4,j}(i)$ in (20a,b), are determined by,

$$Q_{v2,j}(i) = [Q_{I,\ell 1} - f_1(i)\sqrt{\Delta p_{G_1}(i)}]\big|_j, \quad j=1,2,...,6 \tag{22a}$$

$$Q_{v4,j}(i) = [Q_{I,\ell 2} - g_1(i)\sqrt{\Delta p_{G_3}(i)}]\big|_j, \quad j=1,2,...,6 \tag{22b}$$

The actuator displacements $x_{p,j}$ and velocities $v_{p,j}$ represent the outputs of the system, which are determined integrating twice the (20g) and once the (20h), respectively.

III. Impedance Controller Design

Impedance control essentially allows a physical system to emulate another simpler one, assuming the new behaviour is within the capabilities of the physical system. In this section, a model-based impedance control design for a 6-dof electro-hydraulic Stewart platform is developed. The control design strategy presented here involves two control parts, a feedback and a feedforward one. The developed control analysis is based on the system dynamic and hydraulic model; therefore, it is assumed that the dynamic matrix term $\mathbf{M}^*(\mathbf{x})$, and vector terms $\mathbf{V}^*(\mathbf{x},\dot{\mathbf{x}})$, $\mathbf{G}^*(\mathbf{x})$, and $\mathbf{F}^*_{fr}(\dot{\boldsymbol{\ell}})$, see (4), are known.

In the electromechanical domain, actuator Lorentz forces

are proportional to actuator current. This simplifies motion control laws and allows one to achieve second-order error dynamics converging exponentially to zero. However, a simple relationship between force and current does not exist in electrohydraulic systems, we are interested in studying whether such a system can be described by decoupled invariant error dynamics.

A. Feedback Control Scheme

In the model-based impedance approach, a new desired trajectory is computed and derived by an impedance filter. The design of this new trajectory includes a set of impedance parameters, which are responsible for the good behaviour of the tracking performance.

The feedback controller uses mechanism inverse kinematics, for computing desired actuator length trajectories from desired Cartesian trajectories of the moving platform. The actuator error lengths and speeds are fed into the impedance filter. In this scheme, actuator length feedback is used.

A typical response system behaviour is given by a second order system, [14]. The desired behaviour can be extended considering the virtual point position as a time function and including the velocity, acceleration and force error in the control law scheme, in general. The impedance filter approach used for the electrohydraulic servomechanism at hand, is described by,

$$\mathbf{M}_d(\ddot{\boldsymbol{\ell}}_e - \ddot{\boldsymbol{\ell}}_{des}) + \mathbf{B}_d(\dot{\boldsymbol{\ell}}_e - \dot{\boldsymbol{\ell}}_{des}) + \mathbf{K}_d(\boldsymbol{\ell}_e - \boldsymbol{\ell}_{des}) = \mathbf{F}_{env} \quad (23)$$

where $\mathbf{M}_d$ is the desired 6×6 inertia matrix, and $\mathbf{B}_d$, $\mathbf{K}_d$ are the 6×1 damping and stiffness vectors respectively (desired impedance matrix and vector parameters) describing the desired second order behaviour, $\boldsymbol{\ell}_e$ is the new 6×1 desired impedance trajectory vector, which depends on the desired one, $\boldsymbol{\ell}_{des}$, and the contact force, and $\mathbf{F}_{env}$ is a possible 6×1 environment force vector acting on the system, which can be measured by a force sensor and can be approximated by,

$$\mathbf{F}_{env} = \mathbf{K}_{env}(\boldsymbol{\ell}_{env} - \boldsymbol{\ell}) \quad (24)$$

where $\mathbf{K}_{env}$ is a diagonal 6×6 matrix with positive elements, which symbolizes the environment stiffness, and $\boldsymbol{\ell}_{env}$ is a 6×1 vector, which represents a virtual point of the environment.

The model-based impedance control law is introduced by the feedback servovalve currents, $i_{fb,j}$, $j=1,2,...,6$. This loop can include a number of terms depending on the robustness and performance required. Examples include the following feedback laws,

$$\mathbf{i}_{fb} = \mathbf{K}_v(\dot{\boldsymbol{\ell}}_e - \dot{\boldsymbol{\ell}}) + \mathbf{K}_p(\boldsymbol{\ell}_e - \boldsymbol{\ell}) \quad (25a)$$

$$\mathbf{i}_{fb} = \mathbf{K}_v(\dot{\boldsymbol{\ell}}_e - \dot{\boldsymbol{\ell}}) + \mathbf{K}_p(\boldsymbol{\ell}_e - \boldsymbol{\ell}) + \mathbf{K}_f(\mathbf{F}_{e,des} - \mathbf{F}_e) \quad (25b)$$

where $\mathbf{i}_{fb}$ is the 6×1 servovalve current vector, $\mathbf{K}_p$, $\mathbf{K}_v$ and $\mathbf{K}_f$ are 6×6 diagonal matrices, which represent the control gains of the system, $\boldsymbol{\ell}_e$ is determined by (23), $\mathbf{F}_e$ is found subtracting environmental 6×1 force vector from force vector acting on the load of moving platform, and $\mathbf{F}_{e,des}$ is the 6×1 impedance desirable force vector acting on the moving platform. The force vectors $\mathbf{F}_e$ and $\mathbf{F}_{e,des}$ are given respectively by,

$$\mathbf{F}_e = \mathbf{F}_{act} - \mathbf{F}_{env} \quad (26a)$$

$$\mathbf{F}_{e,des} = \mathbf{M}_{pl}(\mathbf{x}(\boldsymbol{\ell}_e)) + \mathbf{V}_{pl}(\mathbf{x}(\boldsymbol{\ell}_e), \dot{\mathbf{x}}(\boldsymbol{\ell}_e, \dot{\boldsymbol{\ell}}_e)) + \mathbf{G}_{pl}(\mathbf{x}(\boldsymbol{\ell}_e)) \quad (26b)$$

where $\mathbf{F}_{act}$ is the 6×1 net actuator output force vector of the Stewart mechanism, see (9). The terms $\mathbf{x}$ and $\dot{\mathbf{x}}$ are determined using the direct kinematics.

Here, the control law given by (25b) is studied. The impedance control law is examined taking into account the servovalve current functions are assumed to be linear functions of the input current, see (13).

B. Feedforward Control Scheme

A feedforward control signal can be added in the control scheme to further reduce deviations from the desired trajectory. This 6×1 current vector must be determined such that the physical plant behaves like the desired system in noncontact and contact regimes. Schematically, the proposed control scheme is depicted in Fig. 6.

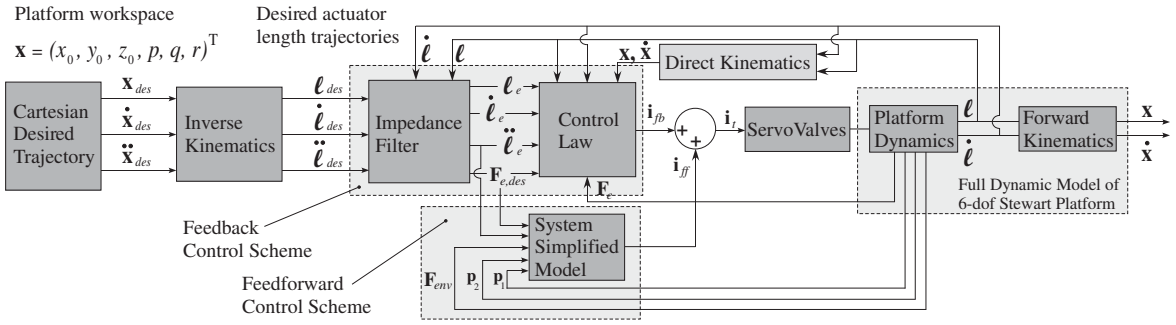

Fig. 6. Schematic view of the full model-based impedance controller diagram of the 6-dof electrohydraulic Stewart mechanism.

The feedforward input servovalve currents are determined using a simplified model of the hydraulic servosystem. The use of a simplified model in the feedforward loop yields practically the same system response as the full model. Moreover, the main advantage of this approach is a significant decrease in the computational power required for simulation.

Using (13)-(17), the feedforward servovalve current vector is determined. For instance, when $i_j > 0$, $j=1,2,...,6$, the components of the feedforward servovalve current vector $\mathbf{i}_{ff} = (i_{ff,1},\ i_{ff,2},...,\ i_{ff,6})^{\mathrm{T}}$ are computed as,

$$i_{ff,j} = \left[\frac{V_t(4\beta_e)^{-1}\Delta\dot{p}_L + (A_1 - A_2)\dot{\ell}}{K_1\sqrt{(p_s - sgn(i)\Delta p_L)/2}} - \frac{K_{0,1}}{K_1}\right]\Bigg|_j, \quad j=1,2,...,6 \quad (27)$$

Finally, the full control law scheme of the 6-dof servo-system is given by the total 6×1 servovalve current vector of the feedback and feedforward current,

$$\mathbf{i}_t = \mathbf{i}_{fb} + \mathbf{i}_{ff} \quad (28)$$

Substituting (28) in (20), an equation of the form of (23) results, which demonstrates the stability of the system. The response is stable provided that the gain matrices are nonnegative, while the error transient depends on the particular gain selection.

IV. Simulation Results

The tracking performance of the controller is evaluated next. The system parameters include the platform mass $m = 300\,\mathrm{kg}$, the moments of inertia about the platform center of mass $I_{xx} = I_{yy} = 25\,\mathrm{kgm}^2$, $I_{zz} = 50\,\mathrm{kgm}^2$, and friction parameters, $b_j = 400\ \mathrm{Ns/m}$, $F_{c0,j} = 50\ \mathrm{N}$ and $F_{s0,j} = 200\ \mathrm{N}$. The ground plan of a 6-6 symmetric Stewart mechanism is illustrated in Fig. 7. The joints of the movable platform and fixed base lie at equal peripheral distances and at radii $r_1 = 0.5\,\mathrm{m}$ and $r_0 = 1.0\,\mathrm{m}$, respectively; the joint distances at the movable platform and fixed base are $d_1 = 0.2\,\mathrm{m}$ and $d_0 = 0.3\,\mathrm{m}$, respectively, see Fig. 7. Further, the valve parameters have been determined as, $K_1 = 1.50\times10^{-5}\,\mathrm{m}^{7/2}/(\mathrm{A\,kg}^{1/2})$ and $K_{0,1} = 5.13\times10^{-9}\,(\mathrm{m}^7/\mathrm{kg})^{1/2}$, see Fig. 4.

Simulations runs were obtained using a number of desired trajectories. As an example, Fig. 8 shows typical simulation results with matrix gain elements $K_{p,j} = 10^3\,A/m$, $K_{v,j} = 3\times10^{-4}\,As/m$, $K_{f,j} = 2\times10^{-6}\,A/N$, $j=1,2,...,6$, and environment stiffness elements $K_{env,j} = 5\times10^4\,\mathrm{N/m}$, $j=1,2,...,6$, while the moving platform raises at Z-direction. A stiff wall is present at $z_{env} = 0.27\ \mathrm{m}$. A desired impedance parameters selection [16] of the system response are $K_{d,j} = 10\,N/m$, $B_{d,j} = 20\,Ns/m$ and $M_{d,j} = 10\,kg$, [16], $j=1,2,...,6$. Finally, the system natural frequencies are determined $\omega_{n,j} = \sqrt{K_{d,j}/M_{d,j}} = 10\,rad/s$, $j=1,2,...,6$. The six servo-actuators follow the same trajectories because of mechanism symmetry. The piston displacement and velocity responses, the environment force response, the input current signals, as well as the servoactuator powers and chamber pressure histories for the actuators are shown in Fig. 8.

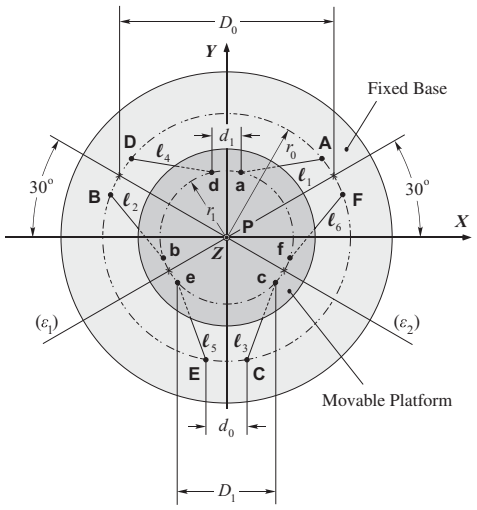

Fig. 7. Ground plan of the considered 6-dof Stewart platform.

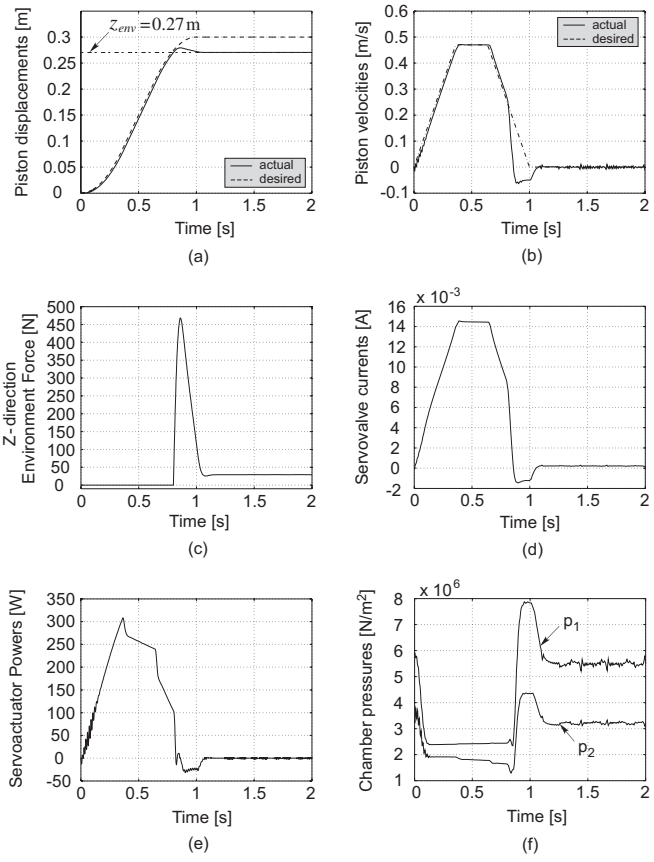

Fig. 8. Simulation results. (a) Piston displacement responses, (b) Piston velocity responses, (c) Environment force response at Z-direction, (d) Input current signals, (e) Actuator power history, (f) Chamber pressure histories.

The robustness of the controller can be demonstrated by applying the controller to the system in the case of parametric errors. For example, assume that the platform load is estimated to be 7% larger than its true value and all joint locations for both the movable platform and fixed base differ by 7% from their true values. Despite these errors, the controller leads the system to the desired location, see Fig. 9.

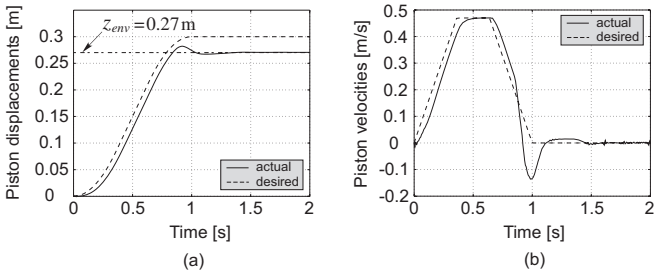

Fig. 9. Simulation results with a parametric error of ± 7%. (a) Piston displacement responses, (b) Piston velocity responses.

V. CONCLUSIONS

The development of a model-based impedance controller for a 6-6 electrohydraulic Stewart platform with symmetric joint locations was studied. Dynamic models were used that described the rigid body equations of the Stewart platform and the hydraulics dynamics of its actuation system. Servovalve models and friction were included in the model. The developed control scheme employed rigid body and actuation dynamics and yielded the servovalve input current vector, in analytical form. The control law consisted of two signals, a feedback and a feedforward signal. An impedance filter modified a desired trajectory according to a specified behaviour. The modified trajectory was fed to the system model to reduce the effects of the nonlinear hydraulic dynamics. The performance of the developed controller was illustrated using typical trajectories. The proposed methodology can be extended to electrohydraulic serial or closed-chain manipulators and simulators.

REFERENCES

[1] V. E. Gough, Discussion in London: Automobile Stability, Control, and Tyre Performance, *In Proceedings of the IMechE's Automobile Division*, 1956, pp. 392-394.

[2] The True Origins of Parallel Robots, Available from: <http://www.parallemic.org>.

[3] D. Stewart, "A platform with six degrees of freedom," *In Proceedings of the IMechE*, Vol. 180, Pt. 1, No 15, 1965-66, pp. 371–385.

[4] L-W. Tsai, *Robot Analysis, The Mechanics of Serial and Parallel Manipulators*, J. Wiley & Sons, 1999.

[5] M. J. Liu, C. X. Li, and C. N. Li, "Generalized Stewart-Gough Platforms and Their Direct Kinematics," *IEEE Transactions on Robotics and Automation*, Vol. 16, No. 1, 2000, pp. 94–98.

[6] X. S. Gao, D. Lei, Q. Liao, and G. F. Zhang, "Generalized Stewart-Gough Platforms and Their Direct Kinematics," *IEEE Transactions on Robotics*, Vol. 21, No. 2, 2005, pp. 141–151.

[7] G. Lebret, K. Liu, and F. L. Lewis, "Dynamic Analysis and Control of a Stewart Platform Manipulator," *Journal of Robotic Systems*, Vol. 10 No. 5, 1993, pp. 629–655.

[8] L-W. Tsai, "Solving the Inverse Dynamics of a Stewart-Gough Manipulator by the Principle of Virtual Work," *Journal of Mechanical Design, Transactions of the ASME*, Vol. 122, 2000, pp. 3–9.

[9] H. E. Merritt, *Hydraulic Control Systems*, J. Wiley, 1967.

[10] M. Jelali, and A. Kroll, *Hydraulic Servosystems: Modelling, Identification and Control*, Springer, 2003.

[11] D. Garagic, and K. Srinivasan, "Application of Nonlinear Adaptive Control Techniques to an Electrohydraulic Velocity Servomechanism," *IEEE Trans. on Control Systems Tech.*, Vol. 12, No. 2, 2004, pp. 303–314.

[12] M. R. Sirouspour, and S. E. Salcudean, "Nonlinear Control of Hydraulic Robots," *IEEE Trans. on Robotics and Automation*, Vol. 17, No. 2, 2001, pp. 173–182.

[13] N. Niksefat, and N. Sepehri, "Robust Force Controller Design for an Electro-Hydraulic Actuator Based on Nonlinear Model," *Proc. 1999 IEEE Int. Conf. Robotics & Automation*, San Francisco, pp. 200–206.

[14] N. Hogan, "Impedance Control: An approach to manipulation: Part I – Theory, Part II – Implementation, Part III – Applications," *ASME Journal of Dynamic Systems, Measurement and Control*, Vol. 107, March 1985, pp. 1-24.

[15] E. D. Fasse, and C. M. Gosselin, "Spatio-Geometric Impedance Control of Gough-Stewart Platforms," *IEEE Transactions on Robotics and Automation*, Vol. 15, No. 2, April 1999, pp. 281-288.

[16] G. Bilodeau, and E. Papadopoulos, "A Model-Based Impedance Control Scheme for High-Performance Hydraulic Joints," *Proc. 1998 Int. Conf. on Intelligent on Robotics & Applications*, Santa Barbara, CA, October 1998.

[17] I. Davliakos, P. Chatzakos, and E. Papadopoulos, "Development of a Model-based Impedance Controller for Electrohydraulic Servos," *Proc. Int. Conf. on Robotics and Applications*, Cambridge, MA, USA, Oct. 31-Nov. 2, 2005.

[18] B. Heinrichs, N. Sepehri, and A.B. Thornton-Trump, "Position-Based Impedance Control of an Industrial Hydraulic Manipulator," *IEEE Control Systems*, February 1997, pp. 46-52.

[19] S. Tafazoli, S. E. Salcudean, K. H. Zaad, and P.D. Lawrence, "Impedance Control of a Teleoperated Excavator," *IEEE Trans. on Control Systems Tech.*, Vol. 10, No. 3, 2002, pp. 355–367.

[20] Q. P. Ha, Q. H. Nguyen, D. C. Rye, and H.F. Durrant-Whyte, "Impedance Control of a hydraulically actuated robotic excavator," *Automation in Construction*, Vol. 9, 2000, pp. 421-435.

[21] B. A. Helouvry, P. Dupont, and C. C. De Wit, "A Survey of Models, Analysis Tools and Compensation Methods for the Control of Machines with Friction," *Automatica*, Vol. 30, No.7, 1994, pp. 1083-1138.

[22] D. Rowell, and D. N. Wormley, *System Dynamics: An Introduction*, Prentice Hall, 1997.

[23] J. F. Blackburn, G. Reethof, and J. L. Shearer, *Fluid Power Control*, Cambridge, MA: MIT Press, 1960.

[24] W. J. Thayer, *Specification Standards for Electrohydraulic Flow Control Servovalves*, Technical Bulletin 117, Moog Incorporation Control Division, E. Aurora, New York, 1962.

[25] I. Davliakos, A. Zafiris, and E. Papadopoulos, "Joint Space Controller Design for Electrohydraulic Servos," *Proc. 2006 IEEE Int. Symp. on Computer-Aided Control Systems Design*, *(CACSD '06)*, October 4-6, 2006, Tech. Universität München, Munich, Germany, pp. 796-801.

[26] R. Rosenberg, and D. Karnopp, *Introduction to Physical System Dynamics*, McGraw Hill, New York, 1983.